Sivaramakrishnan, S., B.G. Thomas, and S.P. Vanka, "Large Eddy Simulation of Turbulent Flow in Continuous Casting of Steel", Materials Processing in the Computer Age III, V. Voller and H. Henein, eds., TMS Annual Meeting, Nashville, TN, March 12-16, 2000, pp. 189-198.

LARGE EDDY SIMULATION OF TURBULENT FLOW IN CONTINUOUS CASTING OF STEEL

S. Sivaramakrishnan, B.G.Thomas and S.P.Vanka

Department of Mechanical and Industrial Engineering
University of Illinois at Urbana Champaign
1206 West Green Street, Urbana IL 61801
Ph: 217-244-5103; Fax: 217-244-6534
email: sivarama@uiuc.edu, bgthomas@uiuc.edu, s-vanka@staff-uiuc.edu

Abstract

During the continuous casting of steel, transient flow events can be very important to the generation of quality problems, such as shear entrainment, surface level fluctuations and bubble entrainment. These phenomena can be better predicted using Large Eddy Simulation (LES) models than the K-ε models, which have been extensively studied. In this work the turbulent transient flow in a water model of a continuous caster has been both simulated using LES models and measured using Particle Image Velocimetry (PIV). The results of PIV and LES have been compared to validate the LES model and also to enhance the understanding of the prominent transient features of the flow field. The flow near the top surface in PIV was found to contain periods of 5-10s when the velocities were three to four times their mean values, which is of importance to the shear entrainment of the liquid flux. In both simulation and PIV the upper roll structure is found to change chaotically from a single large recirculation structure to a set of distinct vortices. The inlet swirl in PIV is seen to persist more than halfway across the mold, causing a characteristic staircase velocity vector pattern when viewed in a plane parallel to the wide faces. The lower rolls in PIV are significantly asymmetric for very long periods of time (~ 1-hour) and go through a repeating sequence of features. One of these features involving a short circuit between the upward and downward flow in the lower roll is also seen in the simulation and is of significance to bubble entrapment.

Introduction

The turbulent flow through the nozzle and in the mold of the continuous caster has been studied extensively using computational Reynolds Averaged Navier Stokes (RANS) flow models [1,2]. Defects, such as internal inclusion of liquid flux through surface shear, pencil pipe defects due to bubble entrapment, surface defects due to level fluctuations are caused by transient flow phenomena occurring in the mold. These phenomena can be better predicted using transient Large Eddy Simulation [3] or "LES" models.

In this paper, experimental results obtained from PIV (Particle Image Velocimetry) measurements, done on a scaled water model are compared with LES models for the same conditions. The comparisons include time averaged velocities, Root Mean Square velocity fluctuations and transient flow features in all parts of the mold. In order to reduce the computational time and resources, some simplifying assumptions were made in the LES models. The comparisons study the validity of these assumptions and also enhance the understanding of prominent transient features of the flow field. This study is being carried out in several stages, involving increasing complexity of the LES models and more detailed PIV studies.

Description of water model and simulation domains

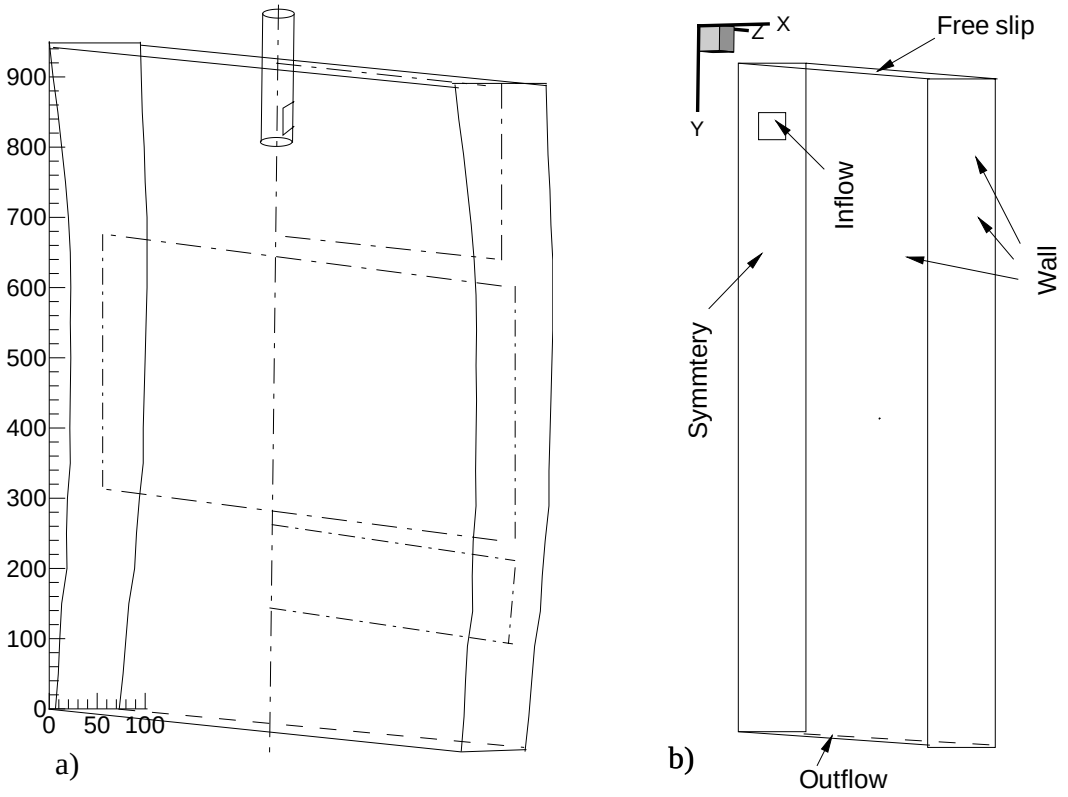

Figure 1: Sketch of water model (a) and simulation domains (b) to scale (All dimensions in mm). The water model domain also shows the three rectangular regions in which PIV data was collected.

Figure 1(a) shows a sketch of the experimental water model of the caster, which is made of transparent Plexiglas. The flow from the tundish passes through a slide gate, which moves at right angles to the wide face. The flow enters the domain through the submerged nozzle and flows out at the bottom, through three pipes attached to circular 35mm diameter outlets in the bottom plate. The experimental domain is nominally symmetric with respect to the centerline shown in the figure. Table I lists the dimensions, flow rates and velocities. The experimental model does not have a constant thickness but tapers from top to bottom, thus simulating only the liquid portion of the steel caster. In order to get good resolution in the PIV measurements, most of the experimental domain is divided into three regions namely the the top region containing the jet and the upper roll, the middle region containing both the lower rolls and the bottom region containing part of the lower roll (Please refer to [4] for a description of the PIV measurement system).

Table I Water model and simulation conditions

No.	Property	Water model	Simulation
1	Length of the model	0.950m	0.956m
2	Thickness of model	Varies from 0.095m at the top to 0.065m	Constant 0.08m
3	Port opening	0.031 x 0.031m	0.031 x 0.031m
4	Top surface	Free surface	Free slip boundary
5	Flow rate through each port	3.528×10^{-4} m^3/s (5.6 gal/min)	3.528×10^{-4} m^3/s (5.6 gal/min)
6	Average inlet velocity	0.4239m/s	0.4239m/s
7	Average jet inlet angle	30^o	30^o
8	Distance of top of port outlet from top surface (submergence depth)	0.075 m (Varies with time)*	0.07207m
9	Outlet	1.5 35mm diameter outlets along each half of the bottom	1.5 35mm square outlets at the bottom
10	Fluid used	Water	Water
11	Kinematic viscosity	1×10^{-6} m^2/s	1×10^{-6} m^2/s
12	Gas flow rate (cubic ft / hr)	0.0	0.0

* An ultrasonic flow sensor is used to record level variation with time. The average water level as recorded by the sensor in this duration is taken as the top surface. Level fluctuations were about 3mm.

Numerical Model

Figure 1 (b) is a plot of the domain used in the simulation. As a first step the flow in the water model is assumed to be symmetric in the large scales; hence only half of it is simulated to reduce computational resources and time. Figure 1 (b) shows the directions of the X, Y and Z axes used. The horizontal velocity component U, is positive towards the narrow face, the vertical velocity component V, is positive in the downward direction and the component in through thickness direction W, is positive into the plane of paper.

The domain is discretized with 128, 184, and 64 points along the X, Y and Z axes respectively meaning a 1.5 million node computational grid. The nozzle inlet consists of 32 and 24 points along the Y and Z axes. The mesh is uniform in the X and Z directions. Along the Y direction, the mesh is uniform at the inlet and is stretched geometrically using a ratio 1.03 in the upward and downward directions. The conservative form of the Navier Stokes equations below is solved to obtain the fluid flow in the domain.

$$\frac{\partial u_j}{\partial x_j} = 0 \qquad (1)$$

$$\frac{\partial u_i}{\partial t} + \frac{\partial}{\partial x_j}(u_i u_j) = -\frac{1}{\rho}\frac{\partial p}{\partial x_i} + \upsilon \frac{\partial^2 u_i}{\partial x_j \partial x_j} \qquad (2)$$

No subgrid scale or other turbulence model is used. The equations are discretized using a fractional step procedure [5] on a staggered grid. Second order central differencing is used for the convection terms and Crank Nicolson scheme [5] is used for the diffusion terms. The Adams-Bashforth fractional step scheme [5] is used to discretize in time with second order accuracy. The implicit diffusion terms are solved for using Alternate Line Inversion. The Pressure Poisson equation is solved using a direct Fast Fourier Transform solver.

Figure 1 (b) also shows the boundary conditions used in the simulation. The inlet for the simulation is obtained by simulating the fully-developed turbulent flow in a square duct [6]. The flow from the exit of the duct is then directed at an angle of 30^o into the simulation inlet.

For parallelization 1-D domain decomposition with MPI (Message Passing Interface) is used. The time step used is 0.001s. The simulations are performed on an Origin 2000 taking 18 CPU s per time step or 13 days (total CPU time) for 60s of flow simulation.

Results and Discussion

Figure 2 shows a side to side comparison of a typical instantaneous vector plot along the center plane of the water model, parallel to the wide faces, obtained from the simulation (a) and PIV measurements (b). Figure 3 compares the corresponding time averaged vector plots. Each side of Figure 3 is made with an equal number of vectors in the X and Y directions. The simulation vector plot is time averaged over 60s.

The PIV vector plot is a composite containing three time-averaged parts. The three parts are the top region containing the upper roll and the jet which has been averaged over 10s (50 snapshots), the middle region containing lower roll (0.25-0.65m below water surface) averaged over 200s (200 snapshots), and the bottom region extending from 0.65m - 0.77m averaged over 40s (200 snapshots). The middle region is also a spatial average of the right and left half regions of the water model, in order to average the considerable differences which arose due to asymmetry between sides. The maximum number of

vectors in a region was reduced 8-fold to 568 in order to maintain good resolution, with 31 along the horizontal and 19 along the vertical in accordance with the camera aperture.

In both the simulation and the experiment, the jet emerges at an angle of approximately 30^o downward. It bends slightly as it traverses the mold to impinge on the narrow face. The flow then splits upward and downward. Due to the high velocity of the jet, a low-pressure region is created in and around the jet resulting in the entrainment of fluid from both above and below. This helps to form the "upper" and "lower" recirculation regions above and below the jet.

The simulation and PIV measurements generally compare very well, both qualitatively and quantitatively. This includes the angle and shape of the jet, upper and lower rolls. Both the measured and simulated velocities in the region near a diagonal from the top-left corner to the center of the upper roll are lower than the velocities up the narrow face and across the water surface. Figure 3 (c) shows velocity vectors in a plane 20 mm from the narrow face which explains the reason for these low velocities in the corner. As seen in the figure, the jet impinges on the narrow face and spreads in all directions. Flow is then stronger up the corners than in the center plane parallel to the wide face. This split flow rejoins close to the top surface, some distance from the narrow face. This leaves an apparent low flow in the region mentioned above.

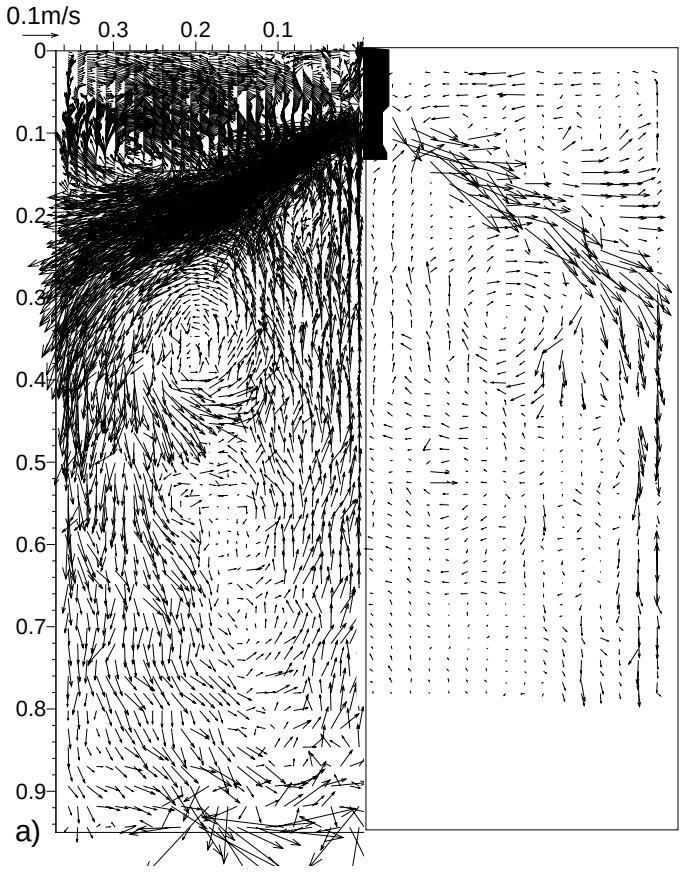

Figure 2: Instantaneous velocity vector plot of (a) simulation and (b) PIV measurement

The PIV jet appears to bend slightly more than the simulation jet as it moves towards the narrow face. The biggest discrepancy, however, is that the upward-moving velocities in the region directly below the SEN in the experiment are smaller than in the simulation.

Figure 4 is a sample plot of time variation of velocity at a point close to the top surface, halfway between the SEN and the narrow face. The PIV points are spaced 0.2s apart as compared to 0.001s increments in the simulation.

The PIV velocity variation shows the existence of two time scales. The lower one is about 0.7s and is predicted well by the simulation.

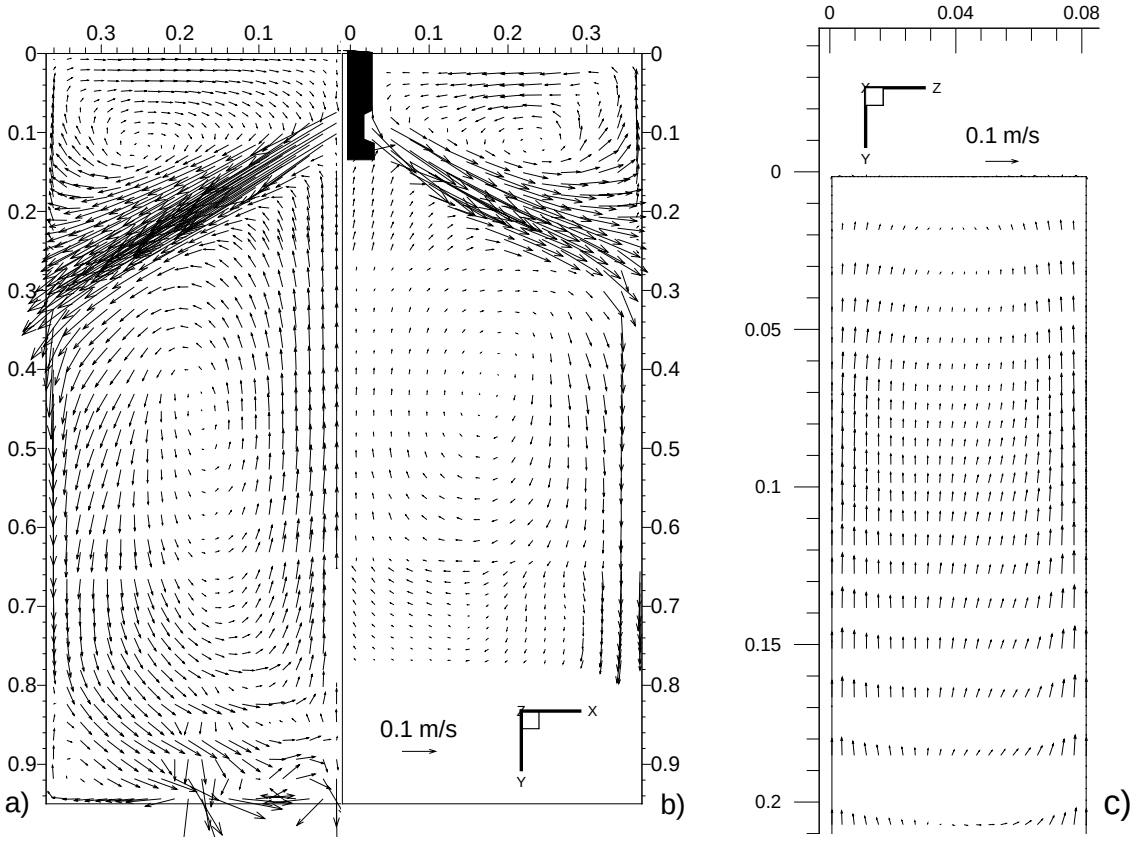

Figure 3: Time averaged velocity vector plot of (a) simulation and (b) PIV; (c) Time averaged velocity vector plot of the simulation parallel to and 20mm from the narrow face.

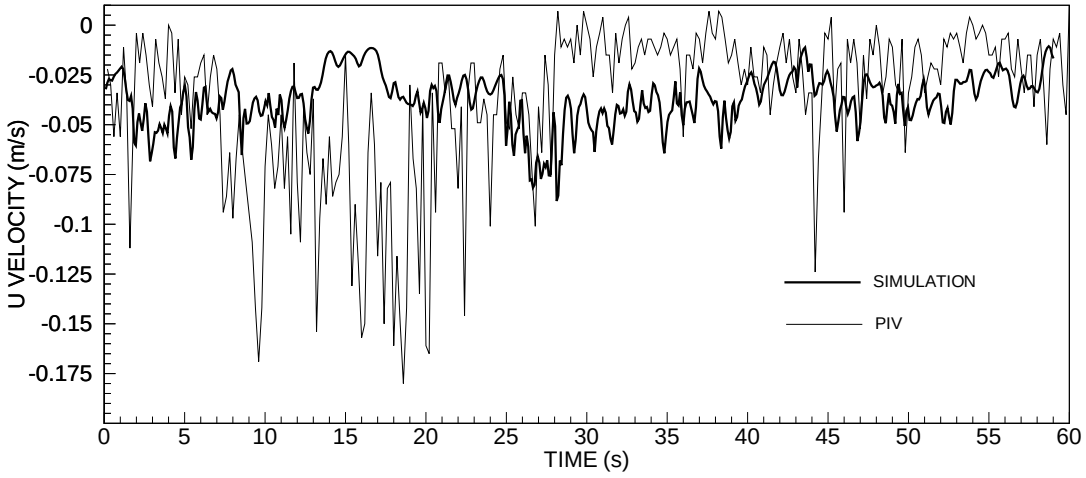

Figure 4: Typical history of U velocity component below the water surface in simulation and PIV.

The higher one is at least 45s and is not seen in the simulation. This results in periods of 5s or more when the velocity close to the top surface is three to four times the mean. This period of high velocity could shear the molten flux layer and cause shear entraiment deep into the caster. These low frequency variations caused by the wide variations in the depth of penetration of the experimental jet are not seen in the simulation.

Figure 5 (a) shows a schematic of the flow from the port that illustrates the swirl. The perpendicular movement of the slide gate flow control positioned high in the nozzle tube, (relative to the wide face) allows flow through only 41% of the nozzle bore area. This causes stronger flow down the inner radius wide face side of the nozzle. This bias in flow over the cross section continues to the nozzle ports. It causes a swirl in the experimental jet [6,7]. The overall jet moves downward at an angle of 30^o and the swirl gradually diffuses. With respect to the jet centerline, the jet moves along a helix, as depicted in the figure.

The swirling experimental jet moves both up and down and in and out of the center plane. As a result of the helical motion, the flow has either an upward or downward component the magnitude depending on the radial location. The in-out motion of the jet results in this vertical component of flow to often occur in the center plane in the PIV measurements. This results in a net instantaneous jet of angle significantly greater than 30^o. Also because of the helix there will be alternate regions where the flow has an angle less than 30^o. This results in a staircase type of pattern as seen in Figure 5 (b).

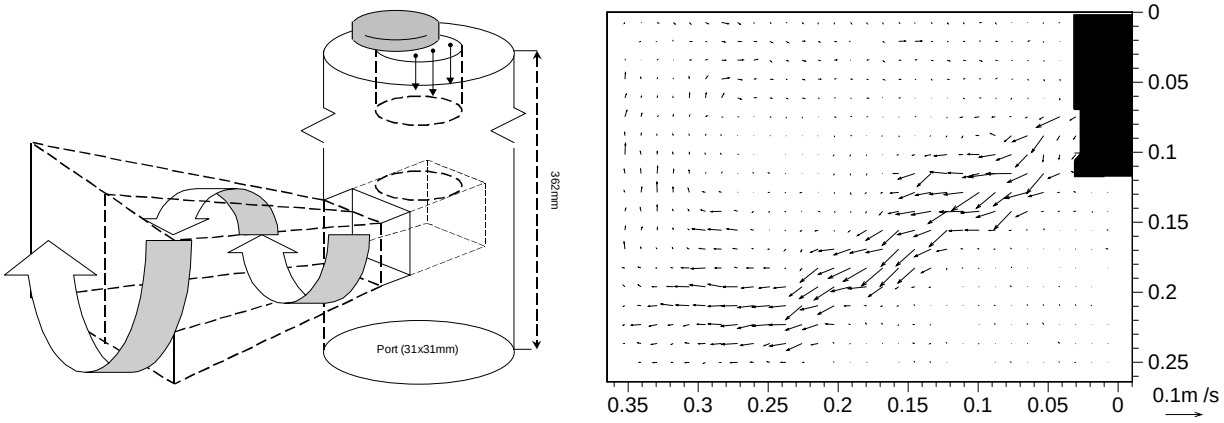

a) b)

Figure 5: (a) Schematic of swirling flow in the PIV jet; (b) The in-out of plane motion of this swirl results in distinct staircase pattern in a instantaneous PIV vector plot of the center plane.

As the jet moves in and out of the center plane at a given point, either the upward or downward moving portion of the spiral flow will be present. This causes the staircase shape to alternate. The time scale of this alternation, and corresponding in-out of plane

motion is of the order of 0.2s. In addition the entire jet chaotically alternates between shallow and deep penetration. The jet also has an in-out motion on a large time scale, resulting in the frequent intermittent disappearance of vectors close to the narrow face, for periods of about 7s. The simulation jet also has miniature staircase patterns which result from jet wobble due solely to turbulence, which is consistent with previous work [8]. However the deviation from 30^o is much smaller than the PIV measurement and the different staircases are out of phase.

This finding implies that the inlet swirl persists more than halfway across the mold. This may significantly affect the flow features in other regions of the mold and explain some of the discrepancies in the results. Thus it is necessary to incorporate the swirling inlet condition along with the in-out of plane motion in future simulations.

Figure 6 is an instantaneous vector plot of the velocities in the top region of the simulation. The upper roll at this instant is seen as a set of distinct vortex structures as opposed to the single large recirculation structure seen in the time average vector plot (Figure 3(a)). The top region alternates chaotically between these two extremes.

Figure 7 is a 30-min time averaged vector plot of the velocities measured in the lower rolls of the water model. Considerable asymmetry can be seen between the left and right rolls, which persist even over this large time period.

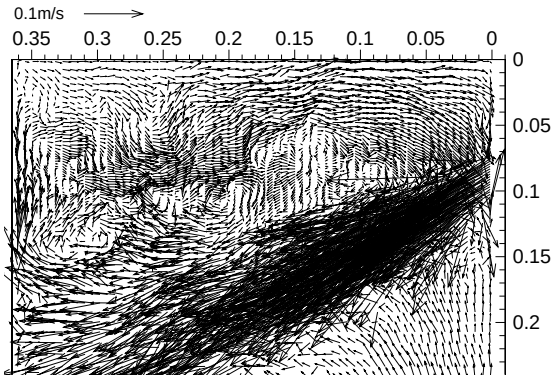

Figure 6: Instantaneous vector plot of the velocities in the top region of the simulation.

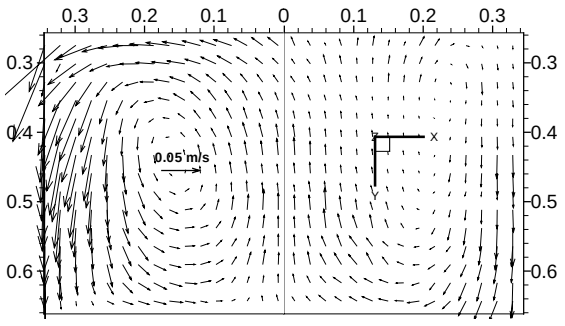

Figure 7: 30 min (2000 snapshots) time averaged vector plot of the velocities in both the lower rolls.

There are two main features of this asymmetry that are especially significant. One is the region of very low velocity below the impingement point on the right, which contrasts with the higher downward flow on the left. This asymmetry was likely caused by an angular misalignment of the nozzle of the order of 1^o in the X-Z plane resulting in the jet on the right moving out of the center plane. Dye injection study for the same configuration, without change in the flow settings is consistent with this angular misalignment. The second is the upward moving flow below the SEN being directed towards the left. This suggests a period of time when the right roll is larger than the left.

Study of the transient flow features over this 30-min. period reveals a repeating sequence of three features when

1) Both rolls are about the same size for about 17s.
2) Right roll is larger than the left for about 30s.
3) A short-circuited structure forms and merges into lower roll over about 14s, while both rolls are about the same size.

The simulation enforces symmetry by simulating only half of the domain with a symmetry boundary condition. The presence of this significant asymmetry necessitates the simulation of both halves of the water model/caster in future work. Figures 2 (a) and (b) show an instant when the short circuit between the upward and downward flows of the lower roll has taken place and the downward motion of the location of the short circuit has begun. The short-circuit of the downward moving flow of the lower roll with the upward moving portion is seen in both experiment and simulation suggesting that it is not caused solely by the input condition but might be caused by intrinsic pressure instabilities or other small disturbances in the turbulent flow field. This phenomenon is important for particle or bubble entrapment and needs to be investigated further.

Conclusions

Both the PIV measurements and simulation together help to get a better understanding of the flow phenomena in the continuous casting process. In particular many transient phenomena have been observed which cannot be simulated using traditional RANS models of turbulent flow.

The inlet condition is of considerable significance to the flow in the mold. The swirl at the port outlet persists until halfway across the mold. The experimental jet has considerable in and out of plane motion, as compared to the simulation, which has an inclined fully-developed turbulent square duct flow as the inlet condition. These two differences together cause the experimental jet to bend so that it impinges nearly horizontally on the narrow face. If the inlet swirl had diffused a short distance from the inlet it would have resulted in closer agreement between simulation and experiment.

The flow near the top surface in the experiment varies by more than 100% of its mean value. This variation consists of a high frequency variation (~1.5 Hz) which is also seen in the simulation. It also consists of a low frequency component (time period of the order of 45s) which results in durations of 5s or more when the horizontal velocities are much larger than the mean values. This component is not seen in the simulation and is speculated to be due to the wide variations in the depth of penetration of the experimental jet not seen in the simulation. This feature is of considerable significance to shear entrainment of the liquid flux.

Although the entire geometry including the inlet nozzle and its port were symmetric, there was considerable, persistent, asymmetry between the two lower rolls. The flow in the lower rolls is not stationary but consists of a sequence of flow phenomena, which repeats chaotically. One of the flow features involving a short-circuit of the downward

moving flow with the upward moving one is seen in both experiment and simulation suggesting that it is not input condition dependent but might be caused by pressure instabilities or other small disturbances in the flow field which are inevitable. This feature is important for particle motion and bubble entrapment, which are responsible for defects in the final product.

Acknowledgements

The authors would like to thank the National Science Foundation (NSF - Grant # DMI - 98-00274) and the Continuous Casting Consortium (CCC) at the University of Illinois at Urbana Champaign (UIUC) for their support of this research, the National Center for Supercomputing Applications (NCSA) at the UIUC for computing time, Dr. Mohammed Assar, Dr Pierre Dauby and the technicians at LTV Steel for their help in the PIV measurements.

References

1) B.G. Thomas, L.J. Mika and F.M. Najjar, “Simulation of fluid flow inside a continuous slab-casting machine”, Metallurgical Transactions B, v 21B, Apr 1990, p 387-400.

2) S.H. Seyedein and M. Hasan, “A three-dimensional simulation of coupled turbulent flow and macroscopic solidification heat transfer for continuous casters”, International Journal of Heat Mass Transfer, v 40, n 18, 1997, p 4405-4423.

3) R.S. Rogallo and Moin. P. “Numerical simulation of turbulent flows”, Ann. Rev. of Fluid Mechanics, v16, 1984, p 99-137.

4) H. Bai and B.G. Thomas, “Two-phase flow in tundish nozzles during continuous casting of steel slabs”, Materials Processing in the Computer Age Symposium, TMS Annual Meeting, Nashville, TN, March 12-16, 2000.

5) J. Tannehill, D. Anderson, R. Pletcher, “Computational Fluid Dynamics and Heat Transfer”, Taylor and Francis, 1997

6) R. Madabushi and S.P. Vanka, “Large eddy simulation of turbulence-driven secondary flow in a square duct”, Physics of Fluids, v 3, n 11, Nov 1991, p 2734-2475.

7) F.M. Najjar, B.G. Thomas and D.E. Hershey, “Numerical study of steady turbulent flow through bifurcated nozzles in continuous casting”, Metallurgical and Materials Transactions B, v 26B, Aug 1995, p 749-765.

8) R.V. Wilson and A.O. Demuren, “Numerical simulation of turbulent jets with rectangular cross section”, ASME Journal of Fluids Engineering, v120, Jun 1998, p 285-290.